Clim. Past Discuss., 10, 2011–2053, 2014
www.clim-past-discuss.net/10/2011/2014/
doi:10.5194/cpd-10-2011-2014

Climate of the Past Discussions
Open Access

Radiative forcings for 28 potential Archean greenhouse gases

B. Byrne and C. Goldblatt

School of Earth and Ocean Sciences, University of Victoria, Victoria, BC, Canada

Received: 2 April 2014 – Accepted: 22 April 2014 – Published: 12 May 2014

Correspondence to: B. Byrne (bbyrne@uvic.ca)

Published by Copernicus Publications on behalf of the European Geosciences Union.

Abstract

Despite reduced insolation in the late Archean, evidence suggests a warm climate which was likely sustained by a stronger greenhouse effect, the so-called Faint Young Sun Problem (FYSP). CO_2 and CH_4 are generally thought to be the mainstays of this enhanced greenhouse, though many other gases have been proposed. We present high accuracy radiative forcings for CO_2, CH_4 and 26 other gases, performing the radiative transfer calculations at line-by-line resolution and using HITRAN 2012 line data for background pressures of 0.5, 1, and 2 bar. For CO_2 to resolve the FYSP alone, 0.21 bar is needed with 0.5 bar of atmospheric pressure, 0.13 bar with 1 bar of atmospheric pressures, or 0.07 bar with 2 bar of atmospheric pressure. For CH_4, we find that near-infrared absorption is much stronger than previously thought, arising from updates to the HITRAN database. CH_4 radiative forcing peaks at 10.3, 9, or 8.3 $W\,m^{-2}$ for background pressures of 0.5, 1 or 2 bar, likely limiting the utility of CH_4 for warming the Archean. For the other 26 HITRAN gases, radiative forcings of up to a few to 10 $W\,m^{-2}$ are obtained from concentrations of 0.1–1 ppmv for many gases. We further calculate the reduction of radiative forcing due to gas overlap for the 20 strongest gases. We recommend the forcings provided here be used both as a first reference for which gases are likely good greenhouse gases, and as a standard set of calculations for validation of radiative forcing calculations for the Archean.

1 Introduction

The standard stellar model predicts that the luminosity of a star increases over its main-sequence lifetime (Gough, 1981). Therefore, the sun is 30 % brighter now than it was when the solar system formed. Despite a dimmer sun during the Archean (3.8–2.5 Gyr BP), geologic evidence suggests surface temperatures similar to today (Donn et al., 1965): this apparent paradox is known as the faint young sun problem (FYSP). To reconcile this, Earth must have had a lower albedo and/or a stronger greenhouse effect

CPD
10, 2011–2053, 2014

in the past. In this work we focus on a stronger greenhouse effect, which is thought to be the primary cause of the warming (Goldblatt and Zahnle, 2011b; Wolf and Toon, 2013). We focus on the late Archean with a solar constant of $0.8 S_0$, resulting in a reduction of $\approx 50\,\mathrm{W\,m^{-2}}$ of insolation.

The most obvious resolution to the FYSP would be higher CO_2 partial pressures. It is believed that the inorganic carbon cycle provides a strong feedback mechanism which regulates the Earth's temperature over geologic timescales (Walker et al., 1981). The rate of silicate weathering (a sink of atmospheric CO_2) is a function of surface temperature which depends on the carbon dioxide partial pressure through the greenhouse effect. Therefore, reduced insolation requires higher atmospheric CO_2 concentrations to regulate the surface temperature and balance the sources (volcanoes) and sinks of atmospheric CO_2. However, geological constraints have been proposed which limit atmospheric CO_2 to levels below those required to keep the early Earth warm (Sheldon, 2006; Driese et al., 2011). Sheldon (2006) used a model based on the mass balance of weathering paleosols and find CO_2 partial pressures between 0.0028–0.026 bar at 2.2 Gyr ago. Driese et al. (2011) use the same method and find CO_2 partial pressures between 0.003 and 0.02 bar at 2.69 Gyr ago. However, these constraints are not uniformly accepted (Kasting, 2013).

Other greenhouse gases likely played an important role in the early Earth's energy budget. Most of the focus has been applied to CH_4 as there are good reasons to expect higher concentrations during the Archean (Zahnle, 1986; Kiehl and Dickinson, 1987; Pavlov et al., 2000; Haqq-Misra et al., 2008; Wolf and Toon, 2013). The Archean atmosphere was nearly anoxic, with very low levels of O_2, which would have increased the photochemical lifetime of methane from 10–12 years today to 1000-10 000 years (Kasting, 2005). The concentration of methane in the Archean is not well constrained but Kasting (2005) suggests that 1–10 ppmv could have been sustained from abiotic sources and up to 1000 ppmv could have been sustained by methanogens. Redox balance models suggest concentrations ≈ 100 ppmv (Goldblatt et al., 2006).

CPD
10, 2011–2053, 2014

Other potential greenhouse gases which have been examined include NH_3 (Sagan and Mullen, 1972; Kuhn and Atreya, 1979; Kasting, 1982; Sagan and Chyba, 1997), hydrocarbons (Haqq-Misra et al., 2008), N_2O (Buick, 2007; Roberson et al., 2011), and OCS (Ueno et al., 2009; Hattori et al., 2011).

Examining the Archean greenhouse involves calculating the radiative effects of greenhouse gases over concentration ranges never before examined. Typically, one time calculations are performed with no standard set of radiative forcings available for comparison. The absence of a standard set of forcings has led to errors going undetected. For example, the warming exerted by CH_4 was significantly overestimated by Pavlov et al. (2000) due to an error in the numbering of spectral intervals (Haqq-Misra et al., 2008) which went undetected for several years.

In previous work, greenhouse gas warming has typically been quantified in terms of the equilibrium surface temperature achieved by running a one-dimensional Radiative-Convective Model (RCM). This metric is sensitive to how climate feedbacks are parametrized in the model and to imposed boundary conditions (e.g. background greenhouse gas concentrations). This makes comparisons between studies and greenhouse gases difficult. It is desirable to document the strengths and relative efficiencies of different greenhouse gases at warming the Archean climate. However, this is near impossible using the literature presently available.

In this study, we use radiative forcing to quantify changes in the energy budget from changes in greenhouse gas concentrations for a wide variety of greenhouse gases. We define radiative forcing as the change in the net flux of radiation at the tropopause due to a change in greenhouse gas concentration with no climate feedbacks. The great utility of radiative forcing is that, to first order, it can be related through a linear relationship to global mean temperature change at the surface (Hansen et al., 2005). It therefore provides a simple and informative metric for understanding perturbations to the energy budget. Furthermore, since radiative forcing is independent of climate response, we get general results which are not affected by uncertainties in the climate

CPD
10, 2011–2053, 2014

response. Radiative forcing has been used extensively to study anthropogenic climate change (IPCC, 2013).

Imposed model boundary conditions significantly affect the warming provided by a greenhouse gas. Boundary conditions that typically vary between studies include: atmospheric pressure, CO_2 concentrations, and CH_4 concentrations. The discrepancies in boundary conditions between studies develop from the poorly constrained climatology of the early Earth. In this work, we examine the sensitivity of radiative forcings to variable boundary conditions.

The atmospheric pressure of the Archean is poorly constrained but there are good theoretical arguments to think it was different from today. For one, the atmosphere is 21 % O_2 by volume today, whereas there was very little oxygen in the Archean atmosphere. Furthermore, there are strong theoretical arguments that suggest that the atmospheric nitrogen inventory was different: large nitrogen inventories exist in the mantle and continents, which are not primordial and must have ultimately come from the atmosphere (Goldblatt et al., 2009). Constraints on the pressure range have recently been proposed, from raindrop imprints (Som et al., 2012) – though this has been challenged (Kavanagh and Goldblatt, 2013), and from noble gas systematics (0.7–1.1 bar, Marty et al., 2013). Atmospheric pressure affects the energy budget in two ways. (1) Increasing pressure increases the moist adiabatic lapse rate, in general suppressing convection and heating the surface and low troposphere at the expense of the upper troposphere. Water concentrations aloft decrease. (2) As the pressure increases, collisions between molecules become more frequent. This results in a broadening of the absorption lines over a larger frequency range. This phenomena is called pressure broadening and generally causes more absorption (Goody and Yung, 1995).

Changes to the concentrations of CO_2 and CH_4 will affect the strength of other greenhouse gases. When multiple gases absorb radiation at the same frequencies, the total absorption is less than the sum of the absorption that each gas contributes in isolation. This difference is known as overlap. It occurs because the absorption is distributed between the gases, so in effect there is less radiation available for each gas to absorb.

CPD
10, 2011–2053, 2014

In this paper, we present calculations of radiative forcings for CO_2, CH_4 and 26 other gases contained in the HIgh-resolution TRANsmission (HITRAN) molecular database for atmospheres with 0.5, 1, and 2 bar of N_2. We aim to provide a complete set of radiative forcing and overlap calculations which can be used as a standard for comparisons. We provide CO_2 and CH_4 radiative forcings over large ranges in concentration. We compare our results with calculations in the literature. For the other 26 HITRAN gases, the HITRAN absorption data is compared with measured cross-sections and discrepancies are documented. Radiative forcings are calculated over a concentrations range of 10 ppbv to 10 ppmv. The sensitivites of the radiative forcings to atmospheric pressure and overlapping absorption with other gases are examined, and our results are compared with results from the literature.

This paper is organized as follows. In Sect. 2, we describe our general methods, evaluation of the spectral data and the atmospheric profile we use. In Sect. 3, we examine the radiative forcings due to CO_2 and CH_4 and examine how our results compare with previous calculations. In Sect. 4, we provide radiative forcings for 26 other gases from the HITRAN database and examine the sensitivity of these results to atmospheric parameters.

2 Methods

2.1 Overview

We calculate absorption cross-sections from HITRAN line parameters and compare our results with measured cross-sections. We develop a single-column atmospheric profile based on constraints of the Archean atmosphere. With this profile, we perform radiative forcing calculations for CO_2, CH_4 and 26 other HITRAN gases.

CPD
10, 2011–2053, 2014

2.2 Spectra

Line parameters are taken from the HITRAN 2012 database (Rothman et al., 2013). We use the LBLABC code, written by David Crisp, to calculate cross-sections from the line data. Line parameters have a significant advantage over measured absorption cross-sections, in that, absorption can be calculated explicitly as a function of temperature and pressure. The strength of absorption lines is a function of temperature and shape is a function of pressure. Neglecting these dependencies can result in significant errors in radiative transfer calculations.

There are, however, some limitations to using HITRAN data. Rothman et al. (2009) explains that the number of transitions included in the database is limited by: (1) a reasonable minimum cutoff in absorption intensity (based on the sensitivity of instruments that observe absorption over extreme terrestrial atmospheric path lengths), (2) lack of sufficient experimental data, or (3) lack of calculated transitions. The molecules for which data are included in the line-by-line portion of HITRAN are mostly composed of small numbers of atoms and have low molecular weights. Large polyatomic molecules have many normal modes of vibration and have fundamentals at very low wavenumbers (Rothman et al., 2009). This makes it difficult to experimentally isolate individual lines of large molecules, so that a complete set of line parameters for these molecules is impossible to obtain.

Computed cross-sections are compared to measured cross-sections from the Pacific Northwest National Laboratory (PNNL) database (Sharpe et al., 2004) for the strongest HITRAN gases (Fig. 1). Where differences exist, it is not straight forward to say which is in error (for example, potential problems with measurments include contamination of samples). Hence we simply note any discrepancy and do our best to note the consequences of these. The largest concentration of the trace gases examined in this work is 10 ppmv, at this concentration only absorption cross-section greater than $\approx 5 \times 10^{-21}$ cm^2 absorb strongly over the depth of the atmosphere.

The similarities and differences between the cross-sections for each gas are:

CPD
10, 2011–2053, 2014

– CH_3OH: the HITRAN line data covers the range of 975–1075 cm^{-1}. In that range the HITRAN cross-sections are an order of magnitude larger than the PNNL cross-sections. Therefore, the PNNL data suggests the concentrations should be an order of magnitude larger to obtain the same forcings as the HITRAN data. PNNL cross-sections indicate that there is missing HITRAN line data over the range 1075–1575 cm^{-1} with peaks of $\approx 5 \times 10^{-20}$ cm^2, which would be optically thick for concentrations $\geq 10^{-6}$ ppv. There is also missing HITRAN data at 550–750 cm^{-1} with peaks of $\approx 5 \times 10^{-21}$ cm^2, which would be optically thick for concentrations $\geq 10^{-5}$ ppv.

– HNO_3: the HITRAN data covers the range of 400–950, 1150–1400, and 1650–1750 cm^{-1}. Over this range, HITRAN and PNNL data agree well except between 725–825 cm^{-1} where the PNNL cross-sections are larger (relevant for concentrations of $\geq 5 \times 10^{-7}$ ppv). PNNL cross-sections indicate that there is significant missing HITRAN line data in the ranges 1000–1150, 1400–1650, and 1750–2000 cm^{-1}, which would be optically thick for concentrations $\geq 5 \times 10^{-6}$ ppv.

– COF_2: the HITRAN cross-sections cover the range of 725–825, 950–1000, 1175–1300, and 1850–2000 cm^{-1}. The PNNL and HITRAN cross-sections agree over this range. HITRAN is missing bands around 650 and 1600 cm^{-1} with peaks of $\approx 10^{-20}$ cm^2, which would be optically thick for concentrations $\geq 5 \times 10^{-6}$ ppv. Additionally, wings of 950–1000, 1175–1300, and 1850–2000 cm^{-1} bands appear missing in HITRAN, relevant at similar concentrations.

– H_2O_2: above 500 cm^{-1}, the HITRAN and PNNL cross-sections cover the same wavenumber range. Over this range, HITRAN cross-sections are about twice the value of the PNNL cross-sections. Therefore, the PNNL data suggests the concentrations should be about twice those of the HITRAN data to obtain the same forcings.

CPD
10, 2011–2053, 2014

- CH_3Br: HITRAN cross-sections are over an order of magnitude greater than the PNNL cross-sections. Therefore, the PNNL data suggests the concentrations should be ≈ 13 times those of the HITRAN data to obtain the same forcings. The PNNL cross-sections indicate missing HITRAN line data over the range of 575–650 cm^{-1} with peaks of $\approx 10^{-20}$ cm^2, which would be optically thick for concentrations $\geq 5 \times 10^{-6}$ ppv.
- SO_2: the HITRAN and PNNL cross-sections agree well except between 550–550 cm^{-1} where HITRAN cross-sections are larger with peaks of $\approx 5 \times 10^{-20}$ cm^2, which would be optically thick for concentrations $\geq 10^{-7}$ ppv.
- NH_3: the HITRAN and PNNL cross-sections agree well.
- O_3: there is no PNNL data for this gas.
- C_2H_2: the HITRAN and PNNL cross-sections agree well.
- HCOOH: the HITRAN data between 1000–1200 and 1725–1875 cm^{-1} agrees with the PNNL data. The PNNL cross-sections indicate missing line data over the range 550–1000 cm^{-1} with peaks of $\approx 5 \times 10^{-19}$ cm^2, which would be optically thick for concentrations $\geq 10^{-8}$ ppv, 1200–1725, and 1875–2000 cm^{-1} with peaks of $\approx 5 \times 10^{-20}$ cm^2, which would be optically thick for concentrations $\geq 10^{-7}$ ppv.
- CH_3Cl: the HITRAN and PNNL cross-sections agree well. PNNL cross-sections indicate missing line data around 600 cm^{-1}.
- HCN: the HITRAN and PNNL cross-sections agree well.
- PH_3: the HITRAN and PNNL cross-sections agree well.
- C_2H_4: the HITRAN data is about an order of magnitude less than PNNL. Therefore, the PNNL data suggests the concentrations should be an order of magnitude less to obtain the same forcings as the HITRAN data.

CPD
10, 2011–2053, 2014

- OCS: the HITRAN and PNNL cross-sections agree well.
- HOCl: there is no PNNL data for this gas.
- N_2O: the HITRAN and PNNL cross-sections agree well.
- NO_2: the HITRAN and PNNL cross-sections agree well in the range 1550–1650 cm^{-1}. The PNNL cross-sections are up to an order of magnitude larger than HITRAN for cross-sections in the range 650–850 cm^{-1} and around 1400 cm^{-1}. PNNL cross-sections indicate missing line data over the ranges 850–1100 and 1650–2000 cm^{-1} with peaks of $\approx 10^{-19}$ cm^2, which would be optically thick for concentrations $\geq 5 \times 10^{-7}$ ppv.
- C_2H_6: the HITRAN and PNNL cross-sections agree well.
- HO_2: there is no PNNL data for this gas.
- ClO: there is no PNNL data for this gas.
- OH: there is no PNNL data for this gas.
- HF: the HITRAN and PNNL data do not overlap. The HITRAN data is available below 500 cm^{-1} and PNNL data is available above $\approx$ 900 cm^{-1}.
- H_2S: the HITRAN and PNNL cross-sections agree well in the range 1100–1400 cm^{-1}. There is no PNNL data for the absorption feature at wavenumbers less that 400 cm^{-1}.
- H_2CO: the HITRAN and PNNL cross-sections agree well for the absorption band in the range 1600–1850 cm^{-1}. The HITRAN data is missing the absorption band over the wavenumber range 1000–1550 cm^{-1} with peaks of $\approx 10^{-20}$ cm^2, which would be optically thick for concentrations $\geq 5 \times 10^{-6}$ ppv.

CPD
10, 2011–2053, 2014

– HCl: there are no optically thick absorption features over the wavenumbers where PNNL data exists.

The spectral data described above only covers the thermal spectrum. HITRAN line parameters are not available for the solar spectrum (other than CO_2, CH_4, H_2O, and O_3). We are unaware of any absorption data for these gases in the solar spectrum. If these gases are strong absorbers in the solar spectrum (e.g. O_3) the radiative forcing calculations could be significantly affected. Very strong heating in the stratosphere would cause dramatic differences in the stratospheric structure which would significantly affect the radiative forcing.

2.3 Atmospheric profile

We perform our calculations for a single-column atmosphere. Performing radiative forcing calculations for a single profile rather than multiple profiles representing the meridional variation in the Earth's climatology introduces only small errors (Myhre and Stordal, 1997; Freckleton et al., 1998; Byrne and Goldblatt, 2014).

The tropospheric temperature structure is dictated largely by convection. We approximate the tropospheric temperature structure with the pseudo-adiabatic lapse rate. The lapse rate is dependent on both pressure and temperature. There is a large range of uncertainty in the surface temperatures of the Archean, we take the surface temperature to be the Global and Annual Mean (GAM) temperature on the modern Earth (289 K). We chose this temperature for two reasons. (1) It makes comparisons with the modern Earth straight forward. (2) It is likely a lower limit for the GAM surface temperature in the Archean. It is thought that temperatures were at-least as warm as present due to the modern glacial climate, given that there is a near-complete absence of evidence of glaciation throughout the Archean (Young, 1991).

We calculate three atmospheric profiles for N_2 inventories of 0.5, 1, and 2 bar. Atmospheric pressure varies with the addition of CO_2 and CH_4. We use the GAM relative

CPD
10, 2011–2053, 2014

humidity from Modern Era Retrospective-analysis for Research and Applications re-analysis data products (Rienecker et al., 2011) over the period 1979 to 2011.

In contrast to the troposphere, the stratosphere (taken to be from the tropopause to the top of the atmosphere) is near radiative equilibrium. The stratospheric temperature structure is therefore sensitive to the concentrations of radiatively active gases. If the stratosphere is optically thin and heated by upwelling radiation, it will be isothermal at the atmospheric skin temperature ($T = (I/(1-\alpha)/8\sigma)^{1/4} \approx 203\,\mathrm{K}$, Pierrehumbert, 2010). We take this to be the case in our calculations. In reality, the stratosphere would not have been optically thin, as CO_2 (and possibly other gases) were likely optically thick for some wavelengths, which would have cooled the stratosphere. Other gases, such as CH_4, may have significantly warmed the stratosphere by absorbing solar radiation. However, the concentrations of these gases are poorly constrained. Since there is no convincing reason to choose any particular profile, we keep the stratosphere at the skin temperature for simplicity. The atmospheric profiles are shown in Fig. 2. We take the tropopause as the atmospheric level at which the pseudoadiabatic lapse rate reaches the skin temperature. Sensitivity tests were performed to examine the sensitivity of radiative forcing to the temperature and water vapour structure. We find that differences in radiative forcing are generally small ($\leq 10\,\%$, Appendix A).

In this study, we explicitly include clouds in our radiative transfer calculations. Following Kasting et al. (1984), many RCMs used to study the Archean climate have omitted clouds, and adjusted the surface albedo such that the modern surface temperatures can be achieved with the current atmospheric composition and insolation. Goldblatt and Zahnle (2011b) showed that neglecting the effects of clouds on longwave radiation can lead to significant over-estimates of radiative forcings, as clouds absorb longwave radiation strongly and with weak spectral dependence. Clouds act as a new surface of emission to the top of the atmosphere and, therefore, the impact on the energy budget of molecular absorption between clouds and the surface is greatly reduced. We take our cloud climatology as cloud fractions and optical depths from International Satellite Cloud Climatology Project D2 data set, averaging from January 1990

CPD
10, 2011–2053, 2014

to December 1992. This period is used by Rossow et al. (2005) and was chosen so that we could compare cloud fractions. We assume random overlap and average by area to estimate cloud fractions. The clouds were placed at 226 K for high clouds, 267 K for middle clouds and 280 K for low clouds, this corresponds to the average temperature levels of clouds on the modern Earth. The cloud climatology of the Archean atmosphere is highly uncertain. Recent GCM studies have found that there may have been less cloud cover due to less surface heating from reduced insolation (Charnay et al., 2013; Wolf and Toon, 2013). Other studies have suggested other mechanisms which could have caused significant changes in cloud cover during the Archean (Rondanelli and Lindzen, 2010; Rosing et al., 2010; Shaviv, 2003) although theoretical problems have been found with all of these studies (Goldblatt and Zahnle, 2011a, b). Nevertheless, given the large uncertainties in the cloud climatology in the Archean the most straight forward assumption is to assume modern climatology, even though there were likely differences in the cloud climatology. Furthermore, the goal of this study is to examine greenhouse forcings and not cloud forcings. Therefore, we want to capture the longwave effects of clouds to a first order degree. Differences in cloud climatology have only secondary effects on the results given here.

Atmospheric profiles are provided as supplementary material. Tables of cloud properties are available as supporting information online for Byrne and Goldblatt (2014).

2.4 Radiative forcing calculations

We use the Spectral Mapping for Atmospheric Radiative Transfer (SMART) code, written by David Crisp (Meadows and Crisp, 1996), for our radiative transfer calculations. This code works at line-by-line resolution but uses a spectral mapping algorithm to treat different wavenumber regions with similar optical properties together, giving significant savings in computational cost. We evaluate the radiative transfer in the range 50–100 000 cm^{-1} (0.1–200 µm) as a combined solar and thermal calculation.

Radiative forcing is calculated by performing radiative transfer calculations on atmospheric profiles with perturbed and unperturbed greenhouse gas concentrations and

CPD
10, 2011–2053, 2014

taking the difference in net flux of radiation at the tropopause. We assume the gases examined here are well-mixed.

3 Results and discussion

3.1 CO_2

We calculate CO_2 radiative forcings up to 1 bar (Fig. 3). At 10 000 ppmv, consistent with paleosol constraints, the radiative forcings are 35 $W m^{-2}$ (2 bar N_2), 26 $W m^{-2}$ (1 bar N_2), and 15 $W m^{-2}$ (0.5 bar N_2), which is considerably short of the forcing required to solve the FYSP, consistent with previous work. The CO_2 forcings given here account for changes in the atmospheric structure due to changes in the N_2 inventory and thus are non-zero at pre-industrial CO_2 for 0.5 and 2 bar of N_2. This results in forcings of about 10 $W m^{-2}$ (2 bar) and -9 $W m^{-2}$ (0.5 bar) at pre-industrial CO_2 concentrations (see Goldblatt et al., 2009, for a detailed physical description).

At very high CO_2 concentrations (> 0.1 bar), CO_2 becomes a significant fraction of the atmosphere. This complicates radiative forcing calculations by changing (1) the atmospheric structure, (2) shortwave absorption/scattering, and (3) uncertainties in the parametrization of continuum absorption. These need careful consideration in studies of very high atmospheric CO_2, so we describe these factors in detail:

1. Large increases in CO_2 increase the atmospheric pressure, and therefore, also increase the atmospheric lapse rate. This results in a cooling of the troposphere and reduction to the emission temperature. Increased atmospheric pressure also results in the broadening of absorption lines for all of the radiatively active gases. Emissions from colder, higher pressure, layers increases radiative forcing.

2. Shortwave radiation is also affected by very high CO_2 concentrations. The shortwave forcing is -2 $W m^{-2}$ at 0.01 bar, -4 $W m^{-2}$ at 0.1 bar and -18 $W m^{-2}$ at 1 bar. There are two separate reasons for this. The smaller affect is absorption

CPD
10, 2011–2053, 2014

of shortwave radiation by CO_2 which primarily affects wavnumbers less than $\approx 10000\,cm^{-1}$ (Fig. 6). The most important effect ($CO_2 > 0.1$ bar) is increased Rayleigh scattering due to the increase in the size of the atmosphere. This primarily affects wavenumbers larger than $\approx 10000\,cm^{-1}$ and is the primary reason for the large difference in insolations through the tropopause between 0.1 and 1 bar of CO_2.

3. There is significant uncertainty in the CO_2 spectra at very high concentrations. This is primarily due to absorption that varies smoothly with wavenumber that cannot be accounted for by nearby absorption lines. This absorption is termed continuum absorption and is caused by the far wings of strong lines and collision induced absorption (CIA) (Halevy et al., 2009). Halevy et al. (2009) show that different parametrizations of line and continuum absorption in different radiative transfer models can lead to large differences in outgoing longwave radiation at high CO_2 concentrations. SMART treats the continuum by using a χ-factor to reduce the opacity of the Voight line shape out to $1000\,cm^{-1}$ from the line center to match the background absorption. We add to this CIA absorption which has been updated with recent results of Wordsworth et al. (2010). We believe that our radiative transfer runs are as accurate as possible given the poor understanding of continuum absorption.

It is worthwhile comparing our calculated radiative forcings with previous results. In most studies, the greenhouse warming from a perturbation in greenhouse gas concentration is quantified as a change of the GAM surface temperature. We convert our radiative forcings to surface temperatures for comparison. This is achieved using climate sensitivity. Assuming the climate sensitivity to be in the range 1.5–4.5 $W\,m^{-2}$ (medium confidence range, IPCC, 2013) for a doubling of atmospheric CO_2 and the radiative forcing for a doubling of CO_2 to be $3.7\,W\,m^{-2}$, we find a range of climate sensitivity parameters of 0.4–1.2 $K(Wm^{-2})^{-1}$ with a best guess of $0.8\,K(Wm^{-2})^{-1}$. We take the

CPD
10, 2011–2053, 2014

CO_2 concentration which gives energy balance at the tropopause (0.13 bar) to be the concentration that gives a surface temperature of 289 K.

The calculated temperature curves are plotted with the results of previous studies (Fig. 4). For all of the studies, surface temperatures were calculated for $0.8S_0$. However there were differences in the atmospheric pressure: von Paris et al. (2008) and Kienert et al. (2012) have 0.77 and 0.8 bar of N_2 respectively, while Haqq-Misra et al. (2008), Wolf and Toon (2013) and Charnay et al. (2013) hold the surface pressure at 1 bar, and remove N_2 to add CO_2.

Model climate sensitivities can be grouped by the type of climate model used. Simple 1-D RCMs (Haqq-Misra et al., 2008; von Paris et al., 2008) have the lowest climate sensitivities (1–4 K). The 3-D models have higher climate sensitivities, but the sensitivities are also more variable between models. Kienert et al. (2012) use a model with a fully dynamic ocean but a statistical dynamical atmosphere. The sea-ice albedo feedback makes the climate highly sensitive to CO_2 concentration and has the largest climate sensitivity ($\approx$ 18.5 K). Charnay et al. (2013) and Wolf and Toon (2013) use models with fully dynamic atmosphere but with simpler oceans. They generally have climate sensitivities between 2.5–4.5 K but Wolf and Toon (2013) find higher climate sensitivities (7–11 K) for CO_2 concentrations of 10 000–30 000 ppmv due to changes in surface albedo (sea ice extent). The climate sensitivities are larger for the 3-D models compared to the RCMs primarily because of the ice-albedo feedback. Variations in climate sensitivity parameters mask variations in radiative forcings.

The concentration of CO_2 required to reach modern day surface temperatures is variable between models. Charnay et al. (2013) and Wolf and Toon (2013) require the least CO_2 to sustain modern surface temperatures (0.06–0.07 bar), primarily because there are less clouds (low and high), the net effect of which is a decrease in albedo. The cloud feedback in these models works as follows: the reduced insolation results in less surface heating, which results in less evaporation and less cloud formation. The RCM studies require CO_2 concentration very close to our results (0.1–0.2 bar), especially considering differences in atmospheric pressure. Kienert et al. (2012) requires very

CPD
10, 2011–2053, 2014

high CO_2 concentrations (≈ 0.4 bar) to prevent runaway glaciation because of the high sensitivity of the ice-albedo feedback in this model.

3.2 CH_4

We calculate CH_4 radiative forcings up to 10 000 ppmv (Fig. 5). At concentrations greater than 100 ppmv we find considerable shortwave absorption. For an atmosphere with 1 bar of N_2, the absorption of solar radiation in the stratosphere is $\approx 1.4\,W\,m^{-2}$ at 100 ppmv, $\approx 6.7\,W\,m^{-2}$ at 1000 ppmv, and $\approx 20\,W\,m^{-2}$ at 10 000 ppmv. This absorption occurs primarily at wavenumbers less than 11 502 cm^{-1} where HITRAN data is available (Fig. 6). We find much more shortwave absorption here than in studies from Jim Kasting's group (Pavlov et al., 2000; Haqq-Misra et al., 2008) which also parametrize solar absorption. The reason for this discrepancy is likely due to improvements in the spectroscopic data. We repeated our radiative forcing calculations using HITRAN 2000 line parameters and found only minor differences in the longwave absorption but much less absorption at solar wavelengths (Fig. 7). Figure 8 shows the solar absorption by CH_4 using spectra from the 2000 and 2012 editions of HITRAN. There is a significant increase in shortwave absorption between 5500–9000 cm^{-1} and around 11 000 cm^{-1}.

Very strong shortwave absorption would have a significant effect on the temperature structure of the stratosphere. Strong absorption would lead to strong stratospheric warming which would limit the usefulness of our results. Nevertheless, our calculations indicate that at 100 ppmv of CH_4 the combined thermal and solar radiative forcings are 7.6 $W\,m^{-2}$ (2 bar of N_2), 7.2 $W\,m^{-2}$ (1 bar of N_2), and 6.2 $W\,m^{-2}$ (0.5 bar of N_2) and the thermal radiative forcings are 9.8 $W\,m^{-2}$ (2 bar of N_2), 8.6 $W\,m^{-2}$ (1 bar of N_2), and 6.8 $W\,m^{-2}$ (0.5 bar of N_2). Therefore, excluding the effects of overlap (which are minimal, Byrne and Goldblatt, 2014), the combined thermal and solar radiative forcing due to 1000 ppmv of CO_2 and 100 ppmv of CH_4 are 42.6 $W\,m^{-2}$ (2 bar of N_2), 33.2 $W\,m^{-2}$ (1 bar of N_2) and 21.2 $W\,m^{-2}$ (0.5 bar of N_2), significantly short of the forcings needed to sustain modern surface temperatures. It should be noted that strong solar absorption

CPD
10, 2011–2053, 2014

makes the precise radiative forcing highly sensitive to the position of the tropopause because this is the altitude at which most of the shortwave absorption is occurring. Therefore, small changes in the position of the tropopause result in large changes in the shortwave forcing.

As with CO_2, we compare our CH_4 radiative forcings to values given in literature (Fig. 9). Temperatures are calculated from radiative forcings assuming a surface temperature of 271 K for 0 ppmv of CH_4 and climate sensitivity parameters of 0.4, 0.8 and 1.2 $K W m^{-2}$, and a background CO_2 concentration of 10 000 ppmv. Due to absorption of shortwave radiation, our calculated surface temperatures decrease for concentrations above 1000 ppmv. Results from Pavlov et al. (2000) are included even though they are known to be erroneous as an illustration of the utility of these comparisons. All other studies give similar surface temperatures. However, these studies lack the strong solar absorption from the HITRAN 2012 database. Haqq-Misra et al. (2008) shortwave radiative transfer is parametrized from data which pre-dates HITRAN 2000 and Wolf and Toon (2013) only include CH_4 absorption below 4650 cm^{-1} where changes to the spectra are not significant.

3.3 Trace gases

The chemical cycles of several other greenhouse gases have been studied in the Archean. It has been hypothesized that higher atmospheric concentrations could have been sustained making these gases important for the planetary energy budget. High concentrations of NH_3 (Sagan and Mullen, 1972), C_2H_6 (Haqq-Misra et al., 2008), N_2O (Buick, 2007), and OCS (Ueno et al., 2009) have all been proposed in the Archean. There are many other greenhouse gases in the HITRAN database that have not been studied, whether these gases could have been sustained at radiatively important concentrations is beyond the scope of this paper. Here we quantify the warming these gases could have provided in the Archean, motivated by future proposals of these as warming agents.

CPD
10, 2011–2053, 2014

3.3.1 Radiative forcings

We produce a first order estimate of the relative absorption strength of the HITRAN gases by taking the product of the irradiance produced by a blackbody of 289 K and the absorption cross-sections to get the absorption per molecule of a gas when saturated with radiation (Fig. 10). Using this metric, H_2O ranks as the 11th strongest greenhouse gas, and CO_2 and CH_4 rank 16th and 27th respectively. This demonstrates that many of the HITRAN gases are strong greenhouse gases and that it is conceivable that low concentrations of these gases could have a significant effect on the energy budget.

We calculate the radiative forcings for the HITRAN gases which produce forcings greater than $1\,W\,m^{-2}$ over the range of 10 ppbv to 10 ppmv (Fig. 11), assuming the gases are well-mixed. The radiative forcings are calculated in an atmosphere which contains only H_2O and N_2. Many of the gases reach forcings greater than $10\,W\,m^{-2}$ at concentrations less than 1 ppmv.

We give rough estimates of the expected radiative forcings assuming the PNNL cross-sections are correct for gases for which the HITRAN and PNNL cross-sections disagree. We have made approximate corrections to the forcings as follows. For some gases the shape of the absorption cross-sections were the same but the magnitude was offset. For these gases, we adjust the concentrations required for a given forcing, this was done for CH_3OH (×10), CH_3Br (×13), C_2H_4 (×0.1), and H_2O_2 (×2). Missing spectra was compensated for by adding the radiative forcings from other gases that had similar spectra. For CH_3OH the C_2H_4 forcings were added. For HCOOH we added the HCN forcing. For NO_2 we added the HOCl forcing. For H_2CO we added the PH_3 forcing for a given concentration scaled up an order of magnitude.

There are significant differences in radiative forcing due to different N_2 inventories. The differences in radiative forcing due to differences in atmospheric pressure varies from gas to gas. Generally, the differences in forcing due to differences in atmospheric structure are similar, but the differences due to pressure broadening are more variable. Broadening is most effective for gases which have broad absorption features with highly

CPD
10, 2011–2053, 2014

variable cross-sections because the broadening of the lines covers areas with weak absorption. Such gases include NH_3, HCN, C_2H_2 and PH_3. At 5 ppmv, 55–60 % of the difference in radiative forcing between atmospheres can be attributed to pressure broadening for these gases. Where as, NO_2 and HOCl which have strong but narrow absorption features show the least difference in forcing due to pressure broadening (20–23 %).

3.3.2 Overlap

Here we examine the reduction in radiative forcing due to overlap for gases which reach radiative forcings of 10 $W m^{-2}$ at concentrations less than 10 ppmv. The concentrations of CO_2 and CH_4 are expected to be quite high in the Archean. Trace gases which have absorption bands coincident with the absorption bands of CO_2 and CH_4 will be much less effective at warming the Archean atmosphere.

We examine the effect of overlap on radiative forcing by looking at several cases with varying concentrations of CO_2, CH_4 (Fig. 12), and other trace gases (Fig. 13). The magnitude of overlap can vary substantially between the gases in question. For the majority of gases overlap with CO_2 is the largest. The reduction in forcing is generally between 10–30 % but can be as high as 86 %. The reduction in forcing are largest for HCN (86 %), C_2H_2 (78 %), CH_3Cl (71 %), NO_2 (52 %), and N_2O (33 %) all with 0.01 bar of CO_2. All of these gases have significant absorption bands in the 550–850 cm^{-1} wavenumber region where CO_2 absorbs the strongest. Of particular interest is N_2O which has previously been proposed to have built up to significant concentrations on the early Earth (Buick, 2007). C_2H_2 could also have been produced by a hypothetical early Earth haze, although previous studies have found that it would not build up to radiatively important concentrations (Haqq-Misra et al., 2008).

The reduction in forcing due to CH_4 is generally less than 20 % but can be as high as 33 %. The reductions in forcing are largest for HOCl (33 %), N_2O (32 %), COF_2 (25 %), and H_2O_2 (21 %) all with 100 ppmv of CH_4. All of which have absorption bands in

CPD
10, 2011–2053, 2014

1200–1350 cm^{-1}. As with CO_2, the radiative forcing from N_2O is significantly reduced due to overlap with CH_4, suggesting that N_2O is not a good candidate to produce significant warming on early Earth except at very high concentrations.

We calculate the reduction in radiative forcing due to overlap between trace gases (Fig. 13). There is a large amount of overlap between C_2H_2, CH_3Cl and HCN resulting in a reduction in radiative forcing of ≈ 30 %. All three gases have their strongest absorption bands in the region 700–850 cm^{-1} and have a secondary absorption band in the region 1250–1500 cm^{-1} which are on the edges of the water vapour window. All three gases have significant overlap with CO_2, for an atmosphere with 0.01 bar of CO_2 the reductions in forcing are > 70 %.

Other traces gases with significant overlap are COF_2 and HOCl (37 %) due to coincident absorption bands at ≈ 1250 cm^{-1}, and CH_3OH and PH_3 (30 %) due to coincident absorption around ≈ 1000 cm^{-1}.

3.3.3 Comparison between our results and previous calculations

We compare inferred radiative forcings from prior work to ours using the same method as for CO_2 and CH_4 (Fig. 14).

Inferred C_2H_6 radiative forcings from Haqq-Misra et al. (2008) for a 1 bar atmosphere agree well with our results. Inferred NH_3 from Kuhn and Atreya (1979) for a 0.78 bar atmosphere agree well with our results, although, our results suggest that the results of Kuhn and Atreya (1979) are on the lower end of possible temperature changes. Inferred N_2O from Roberson et al. (2011) for a 1 bar atmosphere agree well with our results. Roberson et al. (2011) perform radiative forcing calculations with CO_2 and CH_4 concentrations of 320 and 1.6 ppmv. Due to overlap this forcing is likely reduced by ≈ 50 % with early Earth CO_2 and CH_4 concentrations of 10 000 and 100 ppmv. Ueno et al. (2009) give a rough estimate of the radiative forcing due to 10 ppmv of OCS to be 60 $W m^{-2}$. In this work we find the forcing to be much less than this (≈ 20 $W m^{-2}$).

CPD
10, 2011–2053, 2014

4 Conclusions

Using the SMART radiative transfer model and HITRAN line data, we have calculated radiative forcings for CO_2, CH_4 and 26 other HITRAN greenhouse gases on a hypothetical early Earth atmosphere. These forcings are available at several background pressures and we account for overlap between gases. We recommend the forcings provided here be used both as a first reference for which gases are likely good greenhouse gases, and as a standard set of calculations for validation of radiative forcing calculations for the Archean. Many of these gases can produce significant radiative forcings at low concentrations. Whether any of these gases could have been sustained at radiatively important concentrations during the Archean requires study with geochemical and atmospheric chemistry models.

Comparing our calculated forcings with previous work, we find that CO_2 radiative forcings are consistent, but find stronger shortwave absorption by CH_4 than previously recorded. This is primarily due to updates to the HITRAN databse at wavenumbers less than 11 502 cm^{-1}. This new result suggests an upper limit to the warming CH_4 could have provided of about 10 $W m^{-2}$ at 500–1000 ppmv, and that increases in CH_4 above this is likely to cause cooling. Amongst the trace gases, we find that the forcing from N_2O was likely overestimated by Roberson et al. (2011) due to underestimated overlap with CO_2 and CH_4, and that the radiative forcing from OCS was greatly overestimated by Ueno et al. (2009).

Appendix A

Sensitivity

Figure A1 shows the fluxes, radiative forcings and percentage difference in radiative forcings for various possible GAM temperature and water vapour profiles for the early Earth. The effect on radiative forcing calculations from varying the stratospheric

CPD
10, 2011–2053, 2014

temperature from 170 to 210 K while the tropopause temperature is kept constant are very small (< 3 %). Varying the tropopause temperature between 170 and 210 K results in larger differences in radiative forcing (< 10 %). Changing the relative humidity effects radiative forcing by less than 5 %. Radiative forcing calculations are sensitive to surface temperature. Increasing or decreasing a 290 K surface temperature by 10 K results in differences in radiative forcing of ≤ 12 %. However, the difference in forcing between 270 and 290 K is much larger (12–25 %).

Supplementary material related to this article is available online at http://www.clim-past-discuss.net/10/2011/2014/cpd-10-2011-2014-supplement.pdf.

Acknowledgements. We thank Ty Robinson for help with SMART and discussions of the theory behind it. Financial support was received from the Natural Sciences and Engineering Research Council of Canada (NSERC) CREATE Training Program in Interdisciplinary Climate Science at the University of Victoria (UVic); a University of Victoria graduate fellowship to B. Byrne and NSERC Discovery grant to C. Goldblatt. This research has been enabled by the use of computing resources provided by WestGrid and Compute/Calcul Canada. We would also like to thank Andrew MacDougall for helpful comments on an earlier draft of the manuscript.

References

Buick, R.: Did the Proterozoic "Canfield Ocean" cause a laughing gas greenhouse?, Geobiology, 5, 97–100, doi:10.1111/j.1472-4669.2007.00110.x, 2007. 2014, 2028, 2030

Byrne, B. and Goldblatt, C.: Radiative forcing at high concentrations of well-mixed greenhouse gases, Geophys. Res. Lett., 41, 152–160, doi:10.1002/2013GL058456, 2014. 2021, 2023, 2027

CPD
10, 2011–2053, 2014

Charnay, B., Forget, F., Wordsworth, R., Leconte, J., Millour, E., Codron, F., and Spiga, A.: Exploring the faint young Sun problem and the possible climates of the Archean Earth with a 3-D GCM, J. Geophys. Res.-Atmos., 118, 10414, doi:10.1002/jgrd.50808, 2013. 2023, 2026, 2042

Domagal-Goldman, S. D., Meadows, V. S., Claire, M. W., and Kasting, J. F.: Using biogenic sulfur gases as remotely detectable biosignatures on anoxic planets, Astrobiology, 11, 419–441, doi:10.1089/ast.2010.0509, 2011.

Donn, W. L., Donn, B. D., and Valentine, W. G.: On the early history of the Earth, Geol. Soc. Am. Bull., 76, 287–306, doi:10.1130/0016-7606(1965)76[287:OTEHOT]2.0.CO;2, 1965. 2012

Driese, S. G., Jirsa, M. A., Ren, M., Brantley, S. L., Sheldon, N. D., Parker, D., and Schmitz, M.: Neoarchean paleoweathering of tonalite and metabasalt: implications for reconstructions of 2.69 Gyr early terrestrial ecosystems and paleoatmospheric chemistry, Precambrian Res., 189, 1–17, doi:10.1016/j.precamres.2011.04.003, 2011. 2013, 2041

Feulner, G.: The faint young sun problem, Rev. Geophys., 50, RG2006, doi:10.1029/2011RG000375, 2012.

Freckleton, R., Highwood, E., Shine, K., Wild, O., Law, K., and Sanderson, M.: Greenhouse gas radiative forcing: Effects of averaging and inhomogeneities in trace gas distribution, Q. J. Roy. Meteorol. Soc., 124, 2099–2127, doi:10.1256/smsqj.55013, 1998. 2021

Goldblatt, C. and Zahnle, K. J.: Faint young Sun paradox remains, Nature, 474, E3–E4, doi:10.1038/nature09961, 2011a. 2023

Goldblatt, C. and Zahnle, K. J.: Clouds and the Faint Young Sun Paradox, Clim. Past, 7, 203–220, doi:10.5194/cp-7-203-2011, 2011b. 2013, 2022, 2023

Goldblatt, C., Lenton, T. M., and Watson, A. J.: Bistability of atmospheric oxygen and the Great Oxidation, Nature, 443, 683–686, doi:10.1038/nature05169, 2006. 2013, 2043

Goldblatt, C., Claire, M. W., Lenton, T. M., Matthews, A. J., Watson, A. J., and Zahnle, K. J.: Nitrogen-enhanced greenhouse warming on early Earth, Nat. Geosci., 2, 891–896, doi:10.1038/ngeo692, 2009. 2015, 2024

Goody, R. and Yung, Y.: Atmospheric Radiation: Theoretical Basis, Oxford University Press, New York, USA, 1995. 2015

Gough, D.: Solar interior structure and luminoscity variations, Sol. Phys., 74, 21–34, doi:10.1007/BF00151270, 1981. 2012

Halevy, I., Pierrehumbert, R. T., and Schrag, D. P.: Radiative transfer in CO_2-rich paleoatmospheres, J. Geophys. Res.-Atmos., 114, D18112, doi:10.1029/2009JD011915, 2009. 2025

CPD
10, 2011–2053, 2014

Hansen, J., Sato, M., Ruedy, R., Nazarenko, L., Lacis, A., Schmidt, G., Russell, G., Aleinov, I., Bauer, M., Bauer, S., Bell, N., Cairns, B., Canuto, V., Chandler, M., Cheng, Y., Del Genio, A., Faluvegi, G., Fleming, E., Friend, A., Hall, T., Jackman, C., Kelley, M., Kiang, N., Koch, D., Lean, J., Lerner, J., Lo, K., Menon, S., Miller, R., Minnis, P., Novakov, T., Oinas, V., Perlwitz, J., Perlwitz, J., Rind, D., Romanou, A., Shindell, D., Stone, P., Sun, S., Tausnev, N., Thresher, D., Wielicki, B., Wong, T., Yao, M., and Zhang, S.: Efficacy of climate forcings, J. Geophys. Res.-Atmos., 110, D18104, doi:10.1029/2005JD005776, 2005. 2014

Haqq-Misra, J. D., Domagal-Goldman, S. D., Kasting, P. J., and Kasting, J. F.: A revised, hazy methane greenhouse for the archean earth, Astrobiology, 8, 1127–1137, doi:10.1089/ast.2007.0197, 2008. 2013, 2014, 2026, 2027, 2028, 2030, 2031, 2042, 2047, 2052

Hattori, S., Danielache, S. O., Johnson, M. S., Schmidt, J. A., Kjaergaard, H. G., Toyoda, S., Ueno, Y., and Yoshida, N.: Ultraviolet absorption cross sections of carbonyl sulfide isotopologues $OC^{32}S$, $OC^{33}S$, $OC^{34}S$ and $O^{13}CS$: isotopic fractionation in photolysis and atmospheric implications, Atmos. Chem. Phys., 11, 10293–10303, doi:10.5194/acp-11-10293-2011, 2011. 2014

IPCC: Climate Change 2013: The Scientific Basis. Contribution of Working Group I to the Fifth Assessment Report of the Intergovernmental Panel on Climate Change, Cambridge University Press, Cambridge, UK and New York, NY, USA, 2013. 2015, 2025

Kasting, J. F.: Stability of ammonia in the primitive terrestrial atmosphere, J. Geophys. Res-Oc. Atm., 87, 3091–3098, doi:10.1029/JC087iC04p03091, 1982. 2014

Kasting, J. F.: Methane and climate during the Precambrian era, Precambrian Res., 137, 119–129, doi:10.1016/j.precamres.2005.03.002, 2005. 2013, 2043

Kasting, J. F.: How was early earth kept warm?, Science, 339, 44–45, doi:10.1126/science.1232662, 2013. 2013

Kasting, J. F., Pollack, J., and Crisp, D.: Effects of high CO_2 levels on surface-temperature and atmospheric oxidation-state of the early Earth, J. Atmos. Chem., 1, 403–428, doi:10.1007/BF00053803, 1984. 2022

Kavanagh, L. and Goldblatt, C.: The Som Palaeobarometry Method: a critical analysis, presented at: 2012 Fall Meeting, 3–7 December, AGU, San Francisco, California, abstract P21B-1719, 2013. 2015

CPD
10, 2011–2053, 2014

Kiehl, J. and Dickinson, R.: A study of the radiative effects of enhanced atmospheric CO_2 and CH_4 on early Earth surface temperatures, J. Geophys. Res.-Atmos., 92, 2991–2998, doi:10.1029/JD092iD03p02991, 1987. 2013, 2047

Kienert, H., Feulner, G., and Petoukhov, V.: Faint young Sun problem more severe due to ice-albedo feedback and higher rotation rate of the early Earth, Geophys. Res. Lett., 39, L23710, doi:10.1029/2012GL054381, 2012. 2026, 2042

Kuhn, W. and Atreya, S.: Ammonia photolysis and the greenhouse effect in the primordial atmosphere of the Earth, Icarus, 37, 207–213, doi:10.1016/0019-1035(79)90126-X, 1979. 2014, 2031, 2052

Marty, B., Zimmermann, L., Pujol, M., Burgess, R., and Philippot, P.: Nitrogen isotopic composition and density of the archean atmosphere, Science, 342, 101–104, doi:10.1126/Science.1240971, 2013. 2015

Meadows, V. and Crisp, D.: Ground-based near-infrared observations of the Venus nightside: the thermal structure and water abundance near the surface, J. Geophys. Res.-Planet, 101, 4595–4622, doi:10.1029/95JE03567, 1996. 2023

Myhre, G. and Stordal, F.: Role of spatial and temporal variations in the computation of radiative forcing and GWP, J. Geophys. Res., 102, 11181–11200, doi:10.1029/97JD00148, 1997. 2021

Pavlov, A., Kasting, J., Brown, L., Rages, K., and Freedman, R.: Greenhouse warming by CH_4 in the atmosphere of early Earth, J. Geophys. Res.-Planet, 105, 11981–11990, doi:10.1029/1999JE001134, 2000. 2013, 2014, 2027, 2028, 2047

Pierrehumbert, R.: Principles of Planetary Climate, Cambridge Univ. Press, New York, 2010. 2022

Rienecker, M. M., Suarez, M. J., Gelaro, R., Todling, R., Bacmeister, J., Liu, E., Bosilovich, M. G., Schubert, S. D., Takacs, L., Kim, G.-K., Bloom, S., Chen, J., Collins, D., Conaty, A., Da Silva, A., Gu, W., Joiner, J., Koster, R. D., Lucchesi, R., Molod, A., Owens, T., Pawson, S., Pegion, P., Redder, C. R., Reichle, R., Robertson, F. R., Ruddick, A. G., Sienkiewicz, M., and Woollen, J.: MERRA: NASA's Modern-Era Retrospective Analysis for Research and Applications, J. Climate, 24, 3624–3648, doi:10.1175/JCLI-D-11-00015.1, 2011. 2022

Roberson, A. L., Roadt, J., Halevy, I., and Kasting, J. F.: Greenhouse warming by nitrous oxide and methane in the Proterozoic Eon, Geobiology, 9, 313–320, doi:10.1111/j.1472-4669.2011.00286.x, 2011. 2014, 2031, 2032, 2052

CPD
10, 2011–2053, 2014

Rondanelli, R. and Lindzen, R. S.: Can thin cirrus clouds in the tropics provide a solution to the faint young Sun paradox?, J. Geophys. Res., 115, D02108, doi:10.1029/2009JD012050, 2010. 2023

Rosing, M. T., Bird, D. K., Sleep, N. H., and Bjerrum, C. J.: No climate paradox under the faint early Sun, Nature, 464, 744–747, doi:10.1038/nature08955, 2010. 2023

Rossow, W., Zhang, Y., and Wang, J.: A statistical model of cloud vertical structure based on reconciling cloud layer amounts inferred from satellites and radiosonde humidity profiles, J. Climate, 18, 3587–3605, doi:10.1175/JCLI3479.1, 2005. 2023

Rothman, L. S., Gordon, I. E., Barbe, A., Benner, D. C., Bernath, P. E., Birk, M., Boudon, V., Brown, L. R., Campargue, A., Champion, J. P., Chance, K., Coudert, L. H., Dana, V., Devi, V. M., Fally, S., Flaud, J. M., Gamache, R. R., Goldman, A., Jacquemart, D., Kleiner, I., Lacome, N., Lafferty, W. J., Mandin, J. Y., Massie, S. T., Mikhailenko, S. N., Miller, C. E., Moazzen-Ahmadi, N., Naumenko, O. V., Nikitin, A. V., Orphal, J., Perevalov, V. I., Perrin, A., Predoi-Cross, A., Rinsland, C. P., Rotger, M., Simeckova, M., Smith, M. A. H., Sung, K., Tashkun, S. A., Tennyson, J., Toth, R. A., Vandaele, A. C., and Vander Auwera, J.: The HITRAN 2008 molecular spectroscopic database, J. Quant. Spectrosc. Ra., 110, 533–572, doi:10.1016/j.jqsrt.2009.02.013, 2009. 2017

Rothman, L. S., Gordon, I. E., Babikov, Y., Barbe, A., Benner, D. C., Bernath, P. F., Birk, M., Bizzocchi, L., Boudon, V., Brown, L. R., Campargue, A., Chance, K., Cohen, E. A., Coudert, L. H., Devi, V. M., Drouin, B. J., Fayt, A., Flaud, J. M., Gamache, R. R., Harrison, J. J., Hartmann, J. M., Hill, C., Hodges, J. T., Jacquemart, D., Jolly, A., Lamouroux, J., Le Roy, R. J., Li, G., Long, D. A., Lyulin, O. M., Mackie, C. J., Massie, S. T., Mikhailenko, S., Mueller, H. S. P., Naumenko, O. V., Nikitin, A. V., Orphal, J., Perevalov, V., Perrin, A., Polovtseva, E. R., Richard, C., Smith, M. A. H., Starikova, E., Sung, K., Tashkun, S., Tennyson, J., Toon, G. C., Tyuterev, V. G., and Wagner, G.: The HITRAN2012 molecular spectroscopic database, J. Quant. Spectrosc. Ra., 130, 4–50, doi:10.1016/j.jqsrt.2013.07.002, 2013. 2017

Sagan, C. and Chyba, C.: The early faint sun paradox: Organic shielding of ultraviolet-labile greenhouse gases, Science, 276, 1217–1221, doi:10.1126/Science.276.5316.1217, 1997. 2014

Sagan, C. and Mullen, G.: Earth and Mars – evolution of atmospheres and surface temperatures, Science, 177, 52–56, doi:10.1126/Science.177.4043.52, 1972. 2014, 2028

CPD
10, 2011–2053, 2014

Sharpe, S., Johnson, T., Sams, R., Chu, P., Rhoderick, G., and Johnson, P.: Gas-phase databases for quantitative infrared spectroscopy, Appl. Spectrosc., 58, 1452–1461, doi:10.1366/0003702042641281, 2004. 2017

Shaviv, N.: Toward a solution to the early faint Sun paradox: a lower cosmic ray flux from a stronger solar wind, J. Geophys. Res.-Space, 108, 1437, doi:10.1029/2003JA009997, 2003. 2023

Sheldon, N.: Precambrian paleosols and atmospheric CO_2 levels, Precambrian Res., 147, 148–155, doi:10.1016/j.precamres.2006.02.004, 2006. 2013

Som, S. M., Catling, D. C., Harnmeijer, J. P., Polivka, P. M., and Buick, R.: Air density 2.7 billion years ago limited to less than twice modern levels by fossil raindrop imprints, Nature, 484, 359–362, doi:10.1038/nature10890, 2012. 2015

Ueno, Y., Johnson, M. S., Danielache, S. O., Eskebjerg, C., Pandey, A., and Yoshida, N.: Geological sulfur isotopes indicate elevated OCS in the Archean atmosphere, solving faint young sun paradox, P. Natl. Acad. Sci. USA, 106, 14784–14789, doi:10.1073/pnas.0903518106, 2009. 2014, 2028, 2031, 2032

von Paris, P., Rauer, H., Grenfell, J. L., Patzer, B., Hedelt, P., Stracke, B., Trautmann, T., and Schreier, F.: Warming the early earth – CO_2 reconsidered, Planet Space Sci., 56, 1244–1259, doi:10.1016/j.pss.2008.04.008, 2008. 2026, 2042

Walker, J., Hays, P., and Kasting, J.: A negative feedback mechanism for the longterm stabilization of Earth's surface temperature, J. Geophys. Res.-Oceans, 86, 9776–9782, doi:10.1029/JC086iC10p09776, 1981. 2013

Wolf, E. T. and Toon, O. B.: Hospitable archean climates simulated by a general circulation model, Astrobiology, 13, 656–673, doi:10.1089/ast.2012.0936, 2013. 2013, 2023, 2026, 2028, 2042, 2047

Wordsworth, R., Forget, F., and Eymet, V.: Infrared collision-induced and far-line absorption in dense CO_2 atmospheres, Icarus, 210, 992–997, doi:10.1016/j.Icarus.2010.06.010, 2010. 2025

Young, G.: The geologic record of glaciation – relevance to the climatic history of Earth, Geosci. Can., 18, 100–108, 1991. 2021

Zahnle, K.: Photochemistry of methane and the formation of hydrocyanic acid (HCN) in the earth's early atmosphere, J. Geophys. Res., 91, 2819–2834, doi:10.1029/JD091iD02p02819, 1986. 2013

CPD
10, 2011–2053, 2014

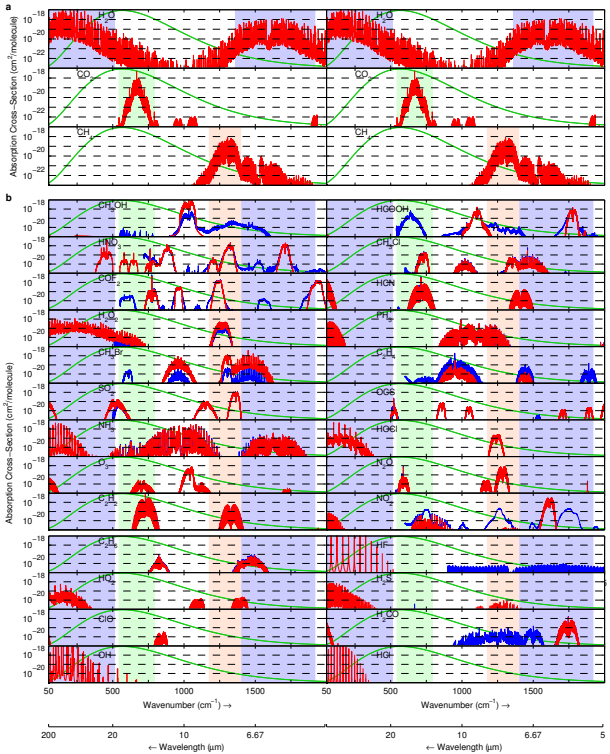

Fig. 1. *Absorption cross-sections.* Absorption cross-sections of **(a)** H_2O, CO_2, and CH_4 and **(b)** potential early Earth trace gases. Cross-sections are calculated from HITRAN line data (red) and measured from the PNNL database (blue) at 1013 hPa and 278 K. The gases are ordered from strongest to weakest based on the analysis in Sect. 3.3 (Fig. 10) in columns from top left to bottom right. Colored shaded areas show wavenumbers at which absorption is strongest for H_2O (blue), CO_2 (green), and CH_4 (red). The green curve shows the shape of the blackbody emissions from a 289 K blackbody.

CPD
10, 2011–2053, 2014

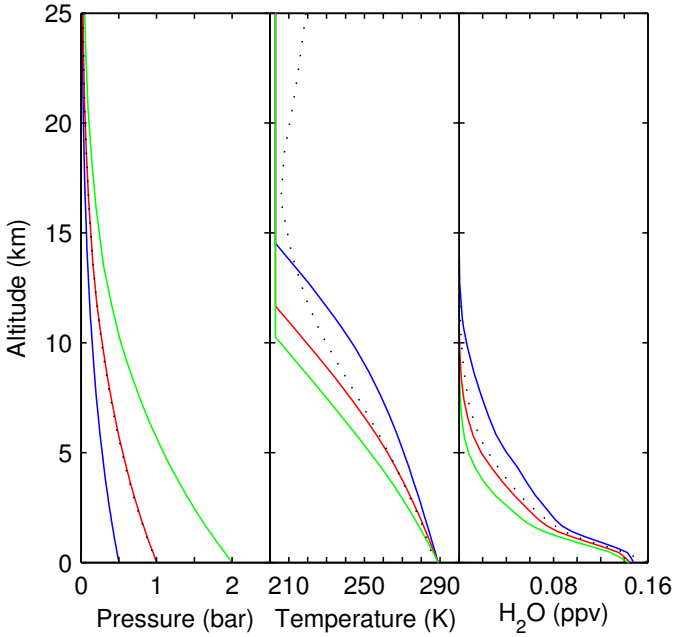

Fig. 2. *Atmospheric Profiles.* Pressure, temperature and water vapor structure of atmospheres with 0.5 bar (blue), 1 bar (red), and 2 bar (green) of N_2. The modern atmosphere is also shown (dotted). The water vapor concentrations are scaled to an atmosphere with 1 bar of N_2.

CPD
10, 2011–2053, 2014

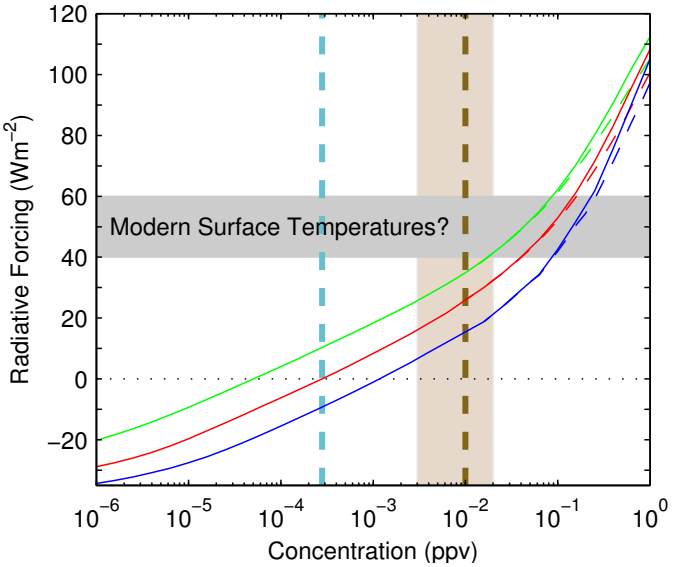

Fig. 3. CO_2 *Radiative Forcings.* Radiative forcing as a function of CO_2 concentration, relative to pre-industrial CO_2 (1 bar N_2). Colors are for atmospheres with 0.5, 1, and 2 bar of N_2. Solid lines are calculated with CIA and dashed lines are calculated without CIA. The shaded region shows the range of CO_2 for the early Earth (3000–20 000 ppmv, Driese et al., 2011). The vertical dashed blue and brown lines give the pre-industrial and early Earth best guess (10 000 ppmv) concentrations of CO_2.

CPD
10, 2011–2053, 2014

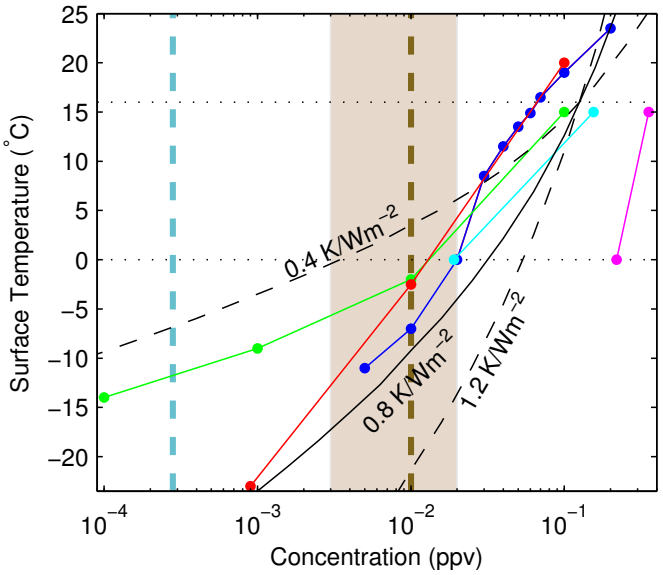

Fig. 4. *Surface temperature as a function of* CO_2 *concentration for* $0.8S_0$. Temperatures are calculated from radiative forcings assuming climate sensitivity parameters of $0.4\,K(Wm^{-2})^{-1}$ (dashed black), $0.8\,K(Wm^{-2})^{-1}$ (solid black) and $1.2\,K(Wm^{-2})^{-1}$ (dashed black) and a surface temperature of 289 K at 0.13 bar of CO_2 (when our model is in energy balance). The results of Wolf and Toon (2013) (blue), Haqq-Misra et al. (2008) (green), Charnay et al. (2013) (red), von Paris et al. (2008) (cyan), and Kienert et al. (2012) (magenta) are also shown.

CPD
10, 2011–2053, 2014

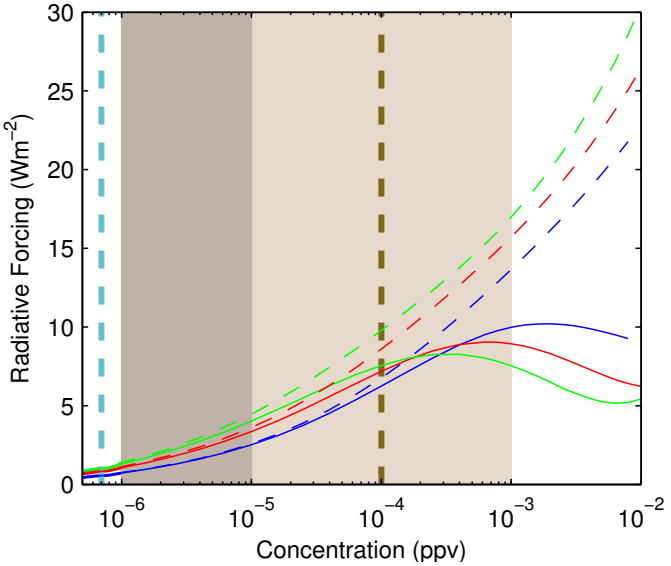

Fig. 5. *Radiative Forcing for* CH_4. Radiative forcing as a function of CH_4 for atmospheres with 0.5 bar (blue), 1 bar (red) and 2 bar (green) of N_2. Dashed curves show the longwave forcing. Shaded region shows the range of CH_4 for the early Earth that could be sustained by abiotic (dark) and biotic (light) sources (Kasting, 2005). The vertical dashed blue and brown lines give the pre-industrial and early earth best guess (100 ppmv, Goldblatt et al., 2006) concentrations of CH_4.

CPD
10, 2011–2053, 2014

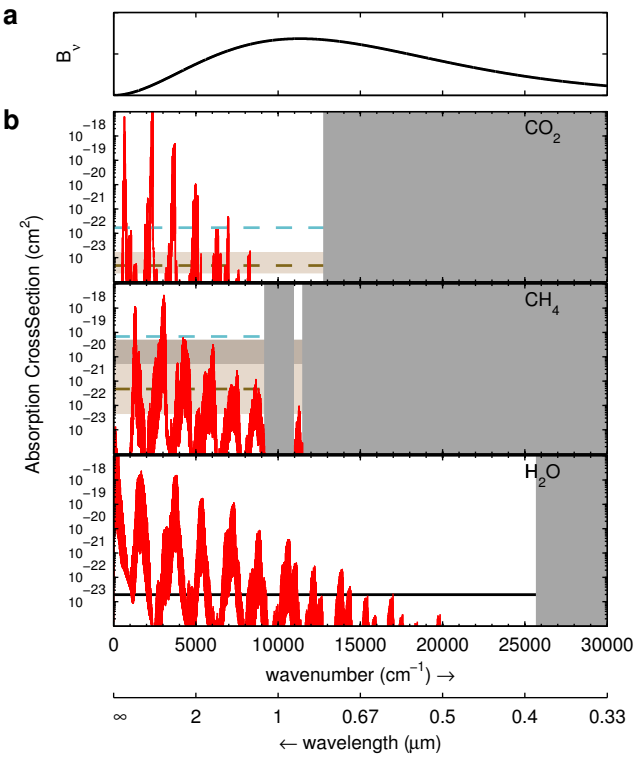

Fig. 6. *Solar absorption cross-sections*. **(a)** Emission spectrum for an object of 5777 K (Effective emitting temperature of modern sun). **(b)** Absorption cross-sections of CO_2, CH_4 and H_2O calculated from line data. Grey shading shows were there is no HITRAN line data. Shaded and dashed lines show absorption cross-sections of unity optical depth for concentrations given in Figs. 3 and 5. Solid black line shows the absorption cross-sections of unity optical depth for H_2O.

CPD
10, 2011–2053, 2014

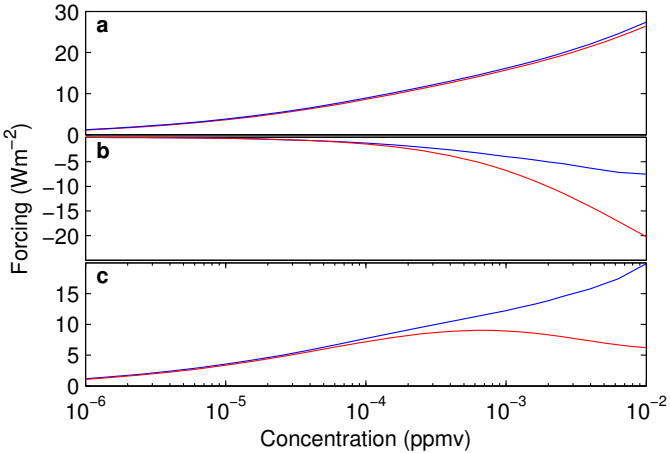

Fig. 7. CH_4 *forcings using HITRAN 2000 and 2012 spectral data.* **(a)** Longwave, **(b)** Shortwave, and **(c)** combined longwave and shortwave radiative forcings using HITRAN 2000 (blue) and 2012 (red) spectral data.

CPD
10, 2011–2053, 2014

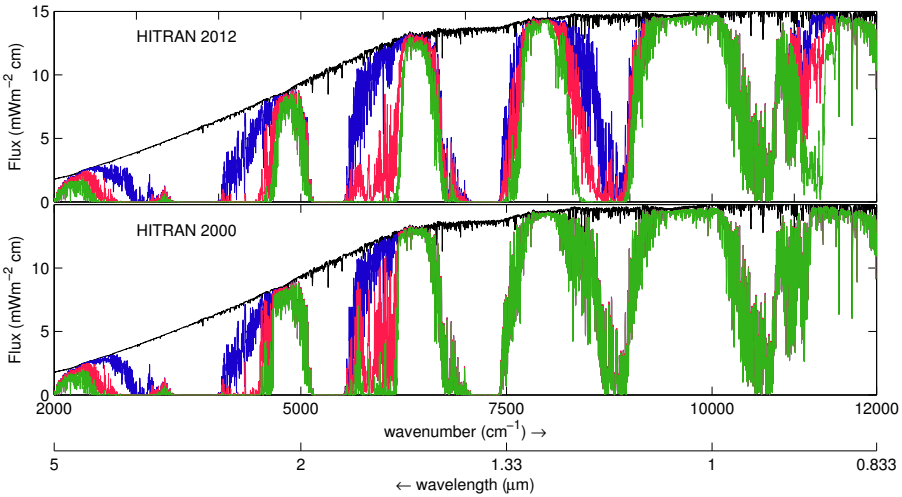

Fig. 8. *Downward shortwave flux.* Insolation at the top of the atmosphere (black) and surface for CH_4 concentrations 1 ppmv (blue), 100 ppmv (red), and 10 000 ppmv (green) using HITRAN 2012 (top panel) and HITRAN 2000 (bottom panel) line data.

CPD
10, 2011–2053, 2014

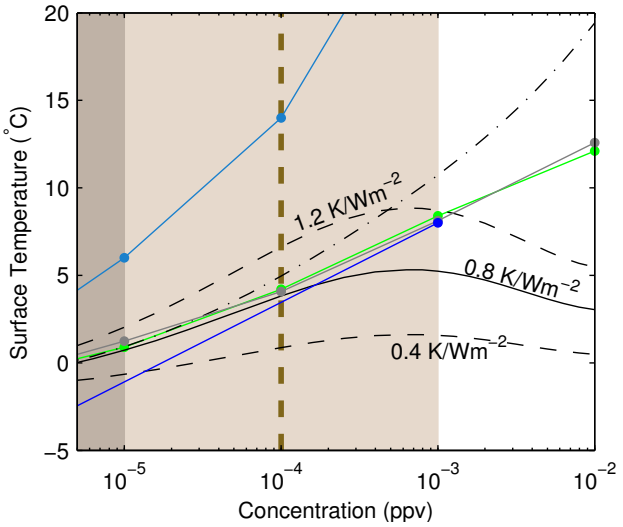

Fig. 9. *Surface temperature as a function of* CH_4 *concentration for* $0.8S_0$. Temperatures are calculated from radiative forcings assuming a surface temperature of 271 K for 0 ppmv of CH_4 and climate sensitivity parameters of 0.4 K$(Wm^{-2})^{-1}$ (dashed black), 0.8 K$(Wm^{-2})^{-1}$ (solid black) and 1.2 K$(Wm^{-2})^{-1}$ (dashed black) and a background CO_2 concentration of 10 000 ppmv. Dashed-dotted black line shows the longwave radiative forcing. The results of Wolf and Toon (2013) (blue), Haqq-Misra et al. (2008) (green), Pavlov et al. (2000) (turquoise), and Kiehl and Dickinson (1987) (grey) are also plotted. Temperatures for Kiehl and Dickinson (1987) are found from radiative forcings assuming a climate sensitivity parameter of 0.81 K$(Wm^{-2})^{-1}$ and a surface temperature of 271 K for 0 ppmv of CH_4.

CPD
10, 2011–2053, 2014

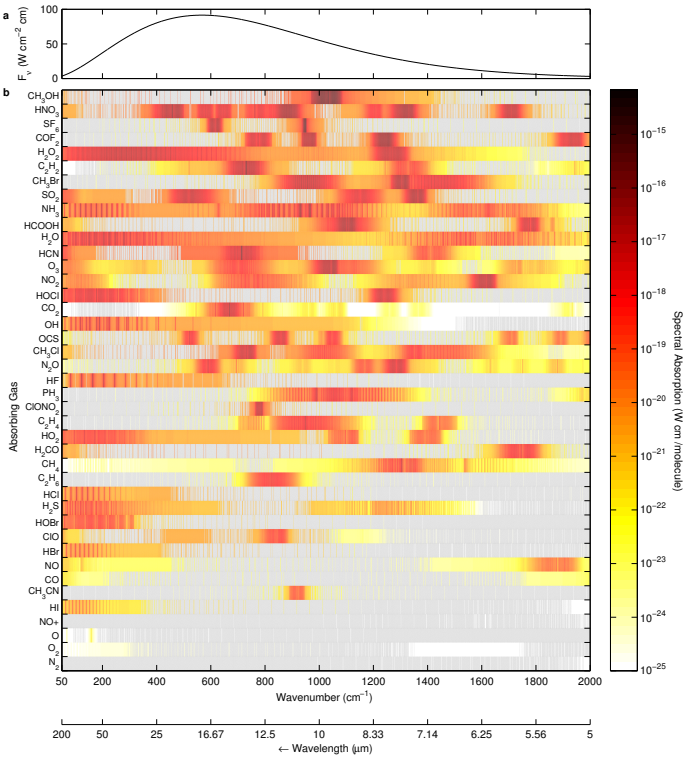

Fig. 10. *Spectral absorption of blackbody emissions.* **(a)** Emission intensity from a blackbody of 289 K. **(b)** Product of emission intensity and absorption cross-sections for gases from the HITRAN 2012 database. Gases are ordered by decreasing spectrum integrated absorption strength from top to bottom. Grey indicates wavenumbers where no absorption data is available. Absorption coefficients were calculated at 500 hPa and 260 K.

CPD
10, 2011–2053, 2014

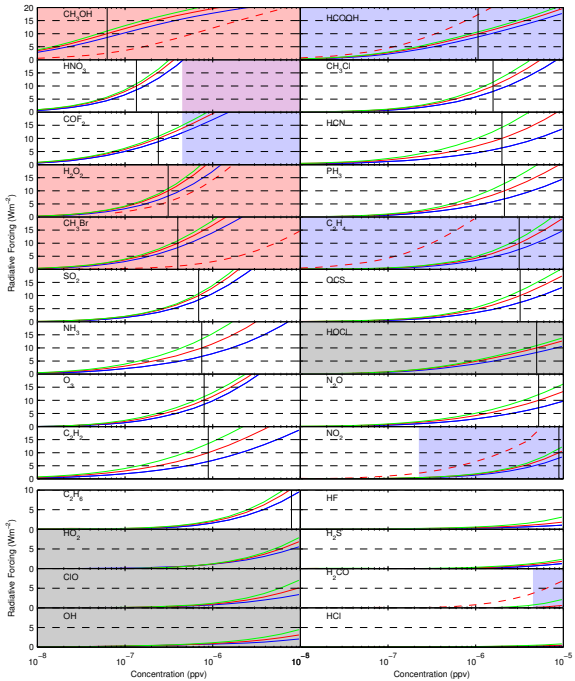

Fig. 11. *Trace gas radiative forcings.* All sky radiative forcings for potential early Earth trace gases, colors are as in Fig. 2. Gases are ordered by the concentration required to get a radiative forcing of 10 W m^{-2}. Shading indicates concentrations where computed cross-sections from HITRAN data were in poor agreement with the PNNL data. The colors indicate areas where HITRAN data underestimates (blue), overestimates (red), or both at different frequencies (purple). Grey shading indicates where no PNNL data was available. Vertical black lines show the concentration at which the radiative forcing is 10 W m^{-2} for a 1 bar atmosphere. Dotted red lines give rough estimates of the radiative forcing accounting for incorrect spectral data. Concentrations are scaled to an atmosphere with 1 bar of N_2.

CPD
10, 2011–2053, 2014

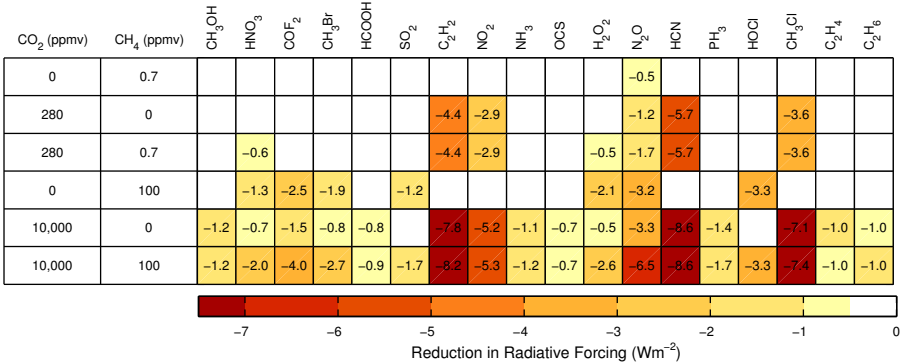

Fig. 12. *Overlap with* CO_2 *and* CH_4. Reduction in radiative forcing due to overlapping absorption. Trace gas concentrations are held at the concentrations which gives a 10 $W m^{-2}$ radiative forcing for an atmosphere with 1 bar of N_2.

CPD
10, 2011–2053, 2014

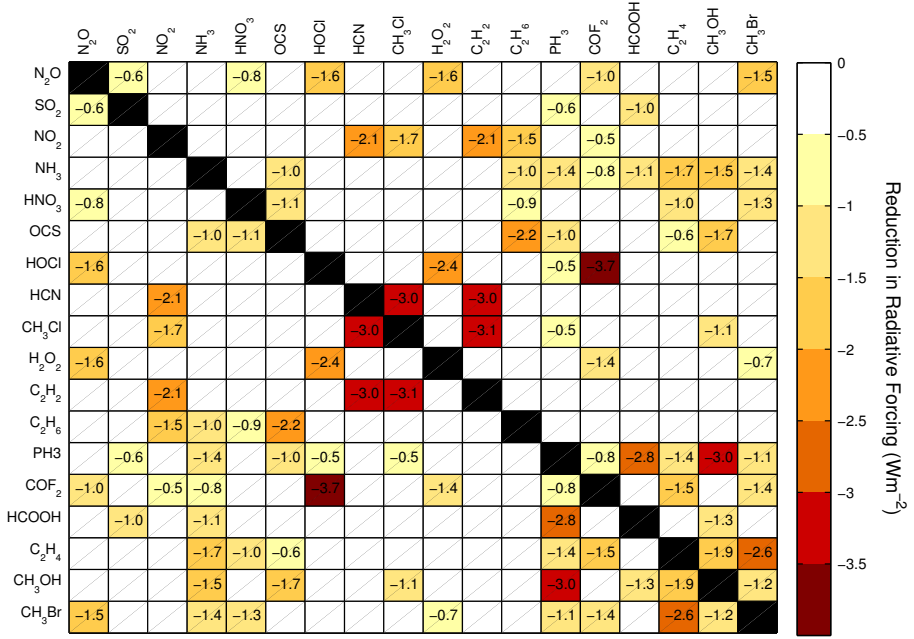

Fig. 13. *Trace gas overlap.* Reduction in radiative forcing due to overlapping absorption. Gas concentrations are held at concentrations which give a 10 $W m^{-2}$ radiative forcing for an atmosphere with 1 bar of N_2.

CPD
10, 2011–2053, 2014

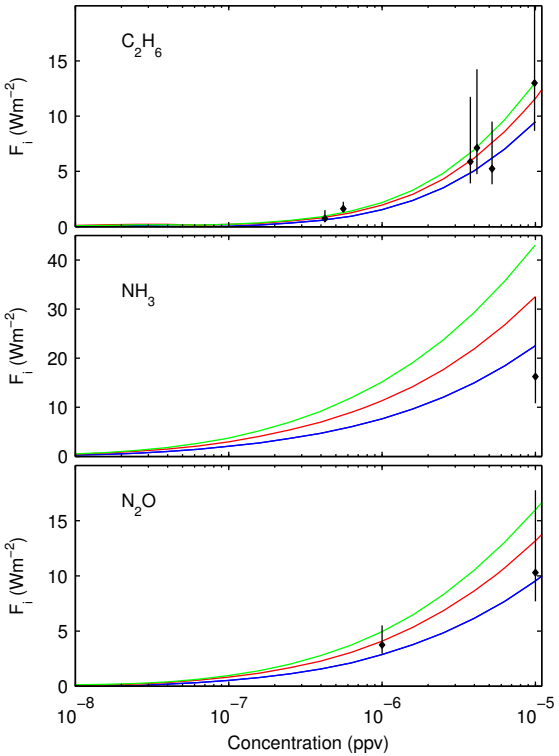

Fig. 14. *Calculated Radiative forcings and inferred radiative forcings from literature.* Literature radiative forcings are inferred from temperature changes reported by Haqq-Misra et al. (2008) (C_2H_6), Kuhn and Atreya (1979) (NH_3) and Roberson et al. (2011) (N_2O). Radiative forcings are calculated assuming a range of climate sensitivity parameters of 0.4 to 1.2 K$(Wm^{-2})^{-1}$ with a best guess of 0.8 K$(Wm^{-2})^{-1}$.

CPD
10, 2011–2053, 2014

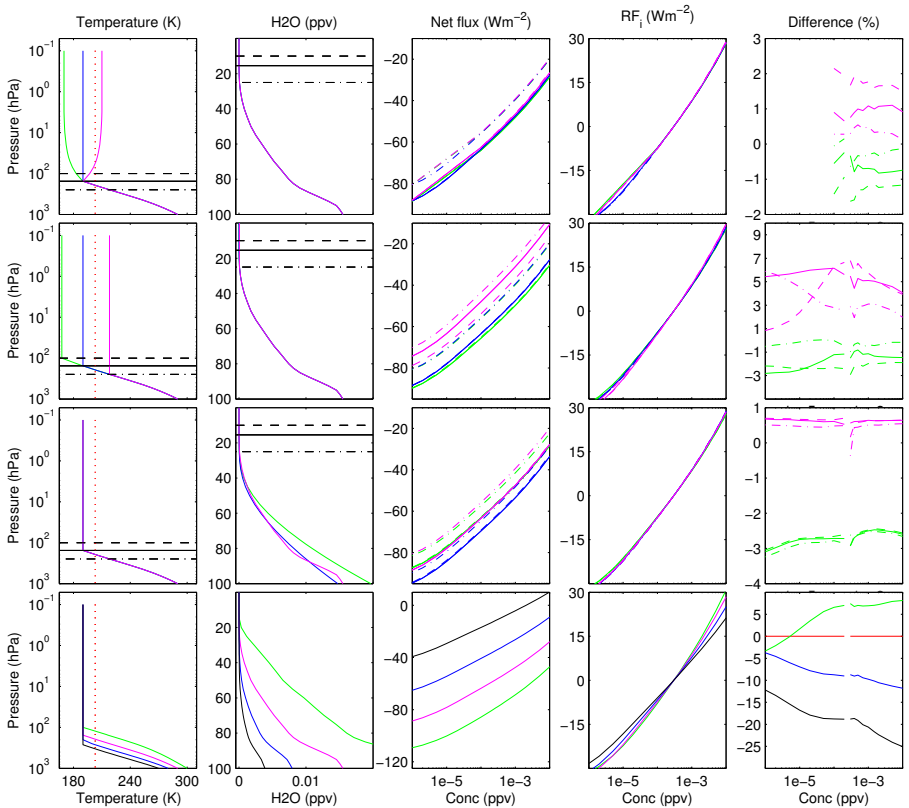

Fig. A1. *Sensitivity Study.* Columns from left to right: Temperature structure, H_2O structure, Net flux of radiation at tropopause, radiative forcing, and percentage difference in radiative forcing. Solid, dashed and dashed-dotted curves represent different tropopause positions. Vertical dotted red line shows the atmospheric skin temperature (203 K).

CPD
10, 2011–2053, 2014